Supporting Information

Digital light processing of 2D lattice composites for tunable self-sensing and mechanical performance

Omar Waqas Saadi[a], Mohammed Ayaz Uddin[a], Andreas Schiffer[a,*], S Kumar[b,*]

[a]Department of Mechanical Engineering, Khalifa University of Science and Technology, Main Campus, P.O. Box 127788, Abu Dhabi, United Arab Emirates

[b]James Watt School of Engineering, University of Glasgow, Glasgow, G12 8LT, UK

* Corresponding authors: andreas.schiffer@ku.ac.ae (A. Schiffer), msv.kumar@glasgow.ac.uk (S. Kumar)

S1. Design of Unit Cells

Table S1. Dimensions (mm) of different unit cells for each choice of relative density $\bar{\rho}$

Type	Dimension	$\bar{\rho} = 20\%$	$\bar{\rho} = 30\%$	$\bar{\rho} = 40\%$
Chiral	Fillet (R)	0.130	0.195	0.263
	Thickness (t)	0.260	0.390	0.525
	Strut length (l_1)	1.11	1.05	0.97
	Strut length (l_2)	2.22	2.10	1.94
	Angle (θ)	45°	45°	45°
Hexagonal	Fillet (R)	0.375	0.564	0.750
	Thickness (t)	0.375	0.564	0.750
	Strut length (l)	1.35	1.03	0.8
	Angle (θ)	120°	120°	120°
Re-entrant	Fillet (R)	0.225	0.340	0.465
	Thickness (t)	0.225	0.340	0.465
	Strut length (l)	1.4	1.36	1.27
	Angle (θ)	75°	75°	75°
Triangular	Fillet (R)	0.045	0.07125	0.095
	Thickness (t)	0.180	0.285	0.380
	Strut length (l)	2.57	2.08	1.68
	Angle (θ)	60°	60°	60°

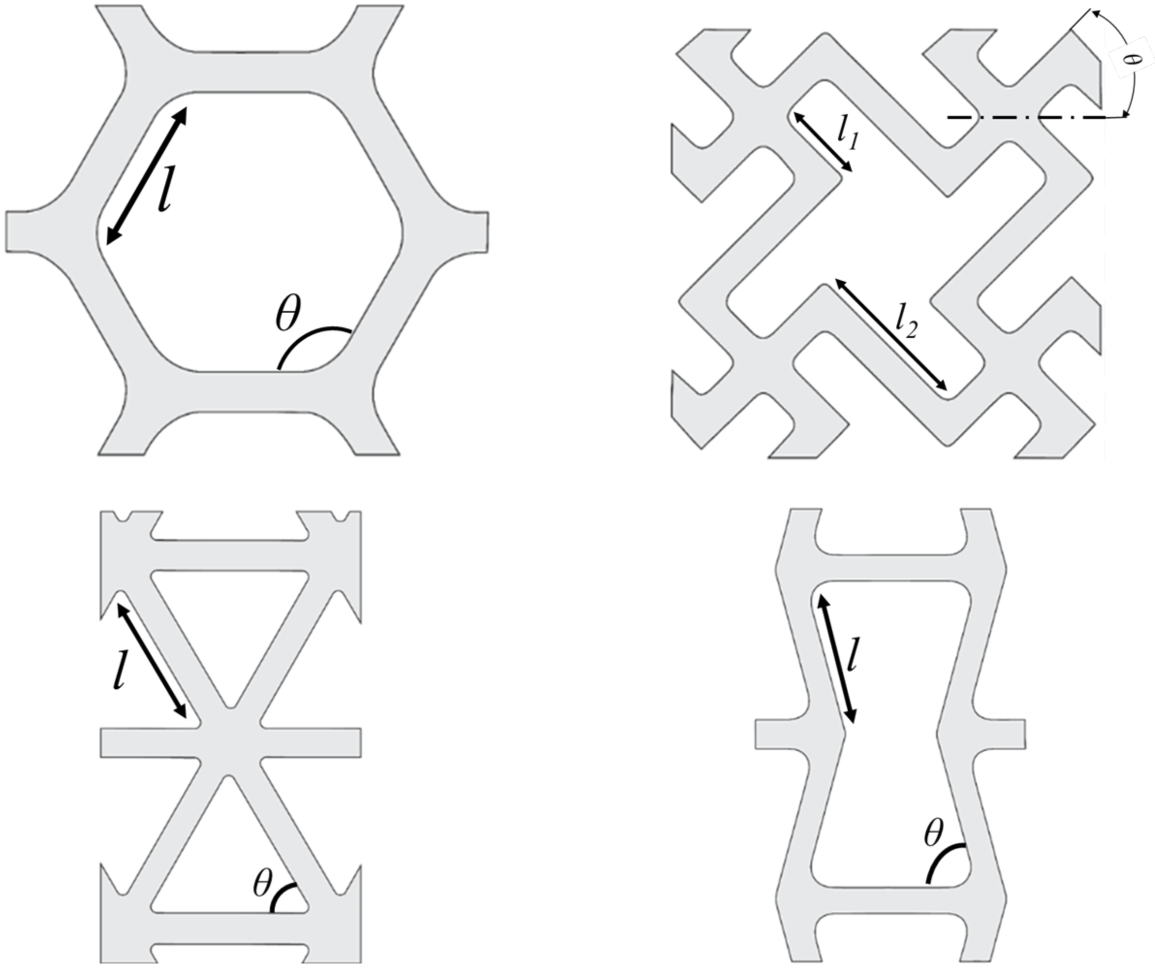

Figure S1. Geometrical parameters that define different of unit cell topologies

S2. Microstructure analysis

High-resolution scanning electron microscopy (SEM) was used to analyze the morphology of the as-received MWCNTs. The SEM scans were performed using a scanning electron microscope (Nova NanoSEM 650, FEI Co., USA) with 7.5 kV accelerating voltage and are shown in Fig. S2. It is clear from the images that the MWCNTs are packed into bundles of variable thickness, forming a complex entangled network.

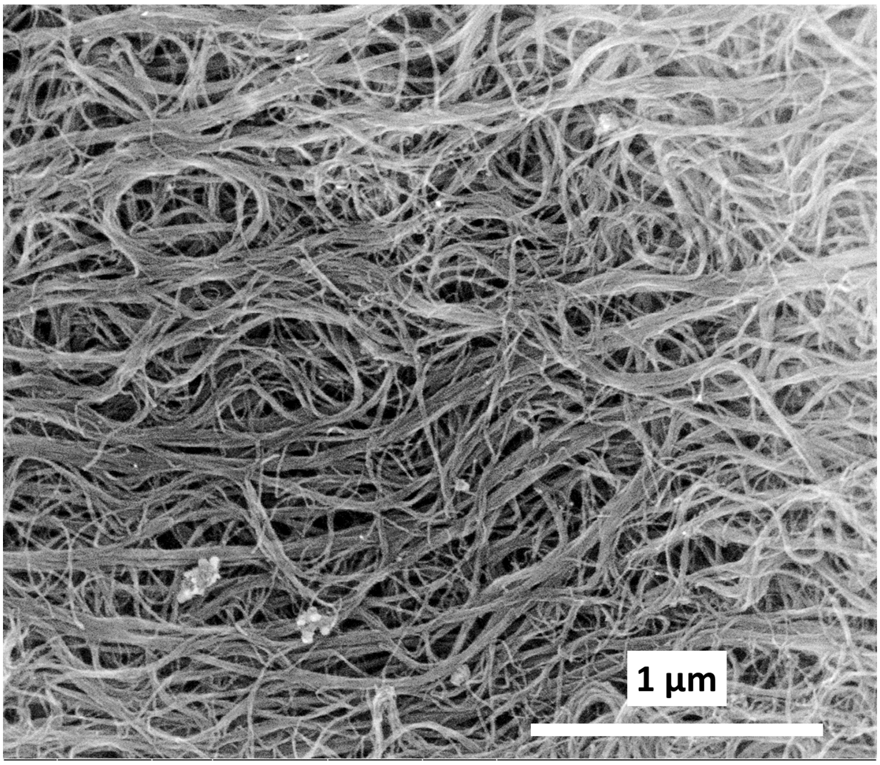

Figure S2. SEM images of the as-received MWCNTs.

S2. Mechanical behavior of 3D printed MWCNT/Plasclear resin

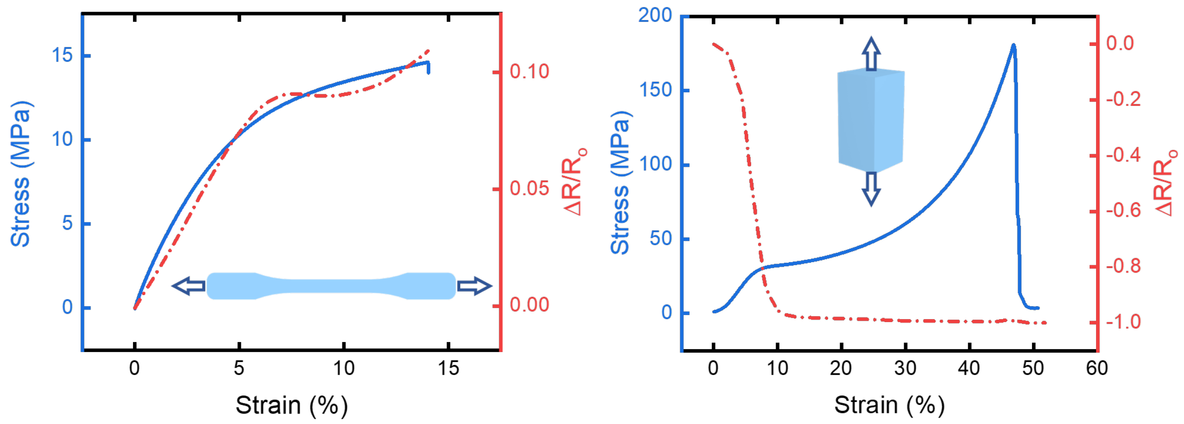

Figure S3. Stress vs. strain (blue) and $\Delta R / R_0$ vs. strain (red) responses of the 3D printed MWCNT/Plasclear nanocomposite with 0.025 phr MWCNT loading under uniaxial (a) tensile and (b) compressive loading.

Table S2. Measured ultimate strength, elastic modulus, failure strain and gauge factor of the 3D printed CNT/Plasclear nanocomposite under uniaxial tensile and compressive loading.

	Tension	**Compression**
Elastic Modulus, E (MPa)	274 ± 3.17	491 ± 32.5
Ultimate Strength, σ_u (MPa)	14.8 ± 0.16	46.1 ± 1.7
Fracture Strain, ε_f (%)	14.2 ±0.99	30*
Gauge Factor, k	1.82 ± 0.24†	-15.8 ± 0.55‡

* Failure strain, ε_d
† $0 \leq \varepsilon \leq 4\%$
‡ $0 \leq \varepsilon \leq 4\%$

Table S3. Summary of mechanical properties of 2D cellular structures obtained from experiments and finite element analysis (FEA)

		Ultimate strength, σ*				Elastic modulus, *E*			
		Hexagonal	Chiral	Triangular	Re-entrant	Hexagonal	Chiral	Triangular	Re-entrant
FEA	$\bar{\rho}$ =20%	0.64	0.11	1.11	1.03	11.1	1.13	38.4	32
	$\bar{\rho}$ =30%	1.24	0.27	2.28	1.83	33	3.99	82.6	66.1
	$\bar{\rho}$ =40%	1.99	0.49	2.95	2.83	65.2	10.6	100.7	123.4
Experiment	$\bar{\rho}$ =20%	0.82	0.092	1.38	1.03	13.26	0.898	39.87	33.11
	$\bar{\rho}$ =30%	1.35	0.33	2.5	1.76	34.1	4.326	71.44	67.04
	$\bar{\rho}$ =40%	1.98	0.51	3.15	2.82	55.8	13.77	89.18	108.3

Table S4. Summary of scaling parameters of the Gibson-Ashby model obtained from least-square fits to the FE predictions and experimental data, respectively.

		$\log(\overline{\boldsymbol{\sigma}})$				$\log(\overline{\boldsymbol{E}})$			
		Hexagonal	Chiral	Triangular	Re-entrant	Hexagonal	Chiral	Triangular	Re-entrant
FEA	y-intercept	-0.244	-0.640	-0.128	-0.165	0.396	-0.148	0.156	0.404
	Slope	1.64	2.16	1.43	1.46	2.56	3.22	1.42	1.94
	Adj. R-Square	0.999	0.999	0.944	0.999	0.998	0.999	0.896	0.994
Experiment	y-intercept	-0.392	-0.438	-0.195	-0.177	0.195	0.374	0.0427	0.199
	Slope	1.27	2.52	1.21	1.44	2.15	4.12	1.26	1.61
	Adj. R-Square	0.999	0.937	0.955	0.993	0.978	0.999	0.991	0.997

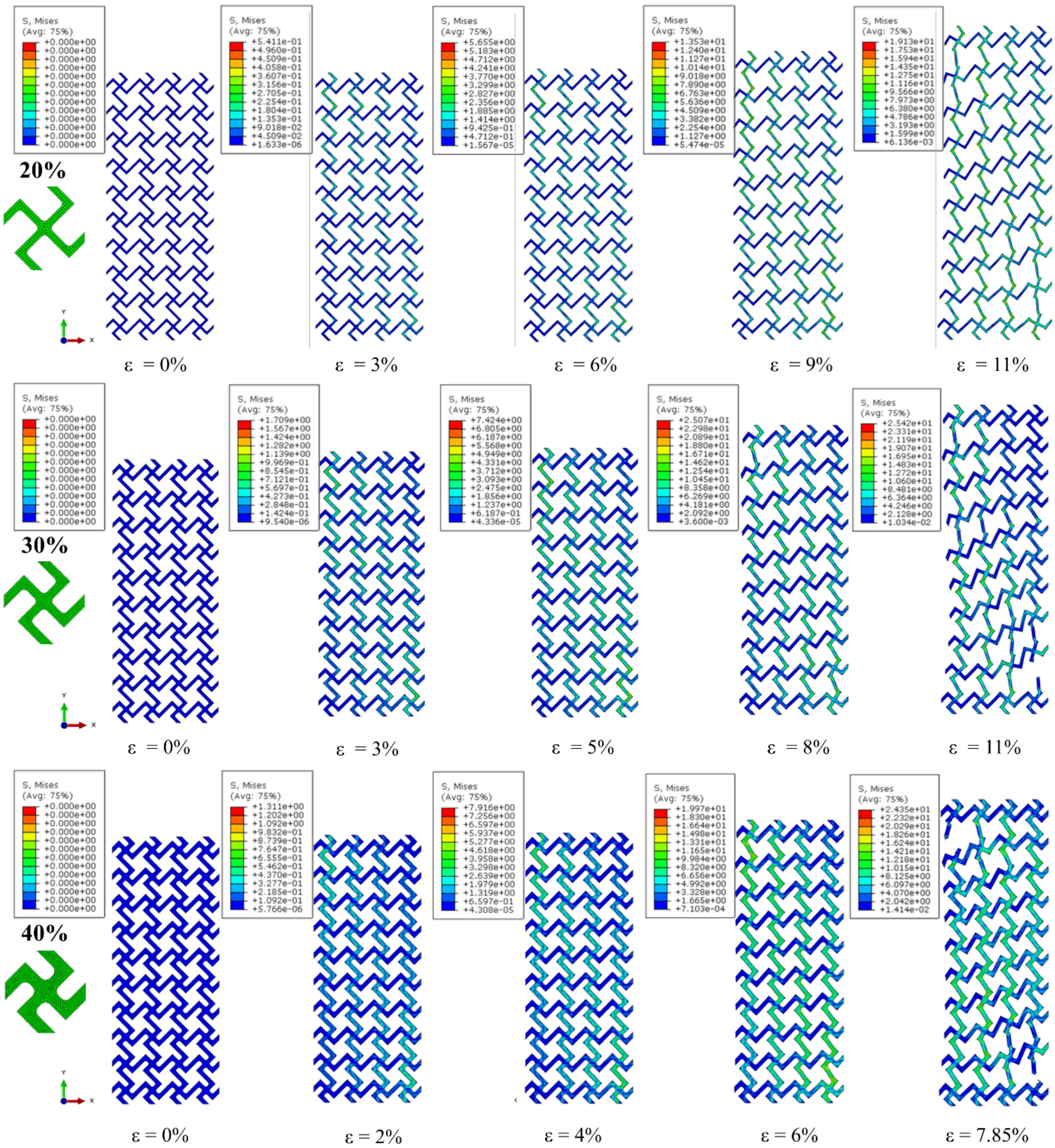

Figure S4. FE contour plots of the von Mises stress (in MPa) induced in the Chiral lattice structures at various levels of tensile strain; results are presented for three choices of relative density (20%, 30%, and 40%).

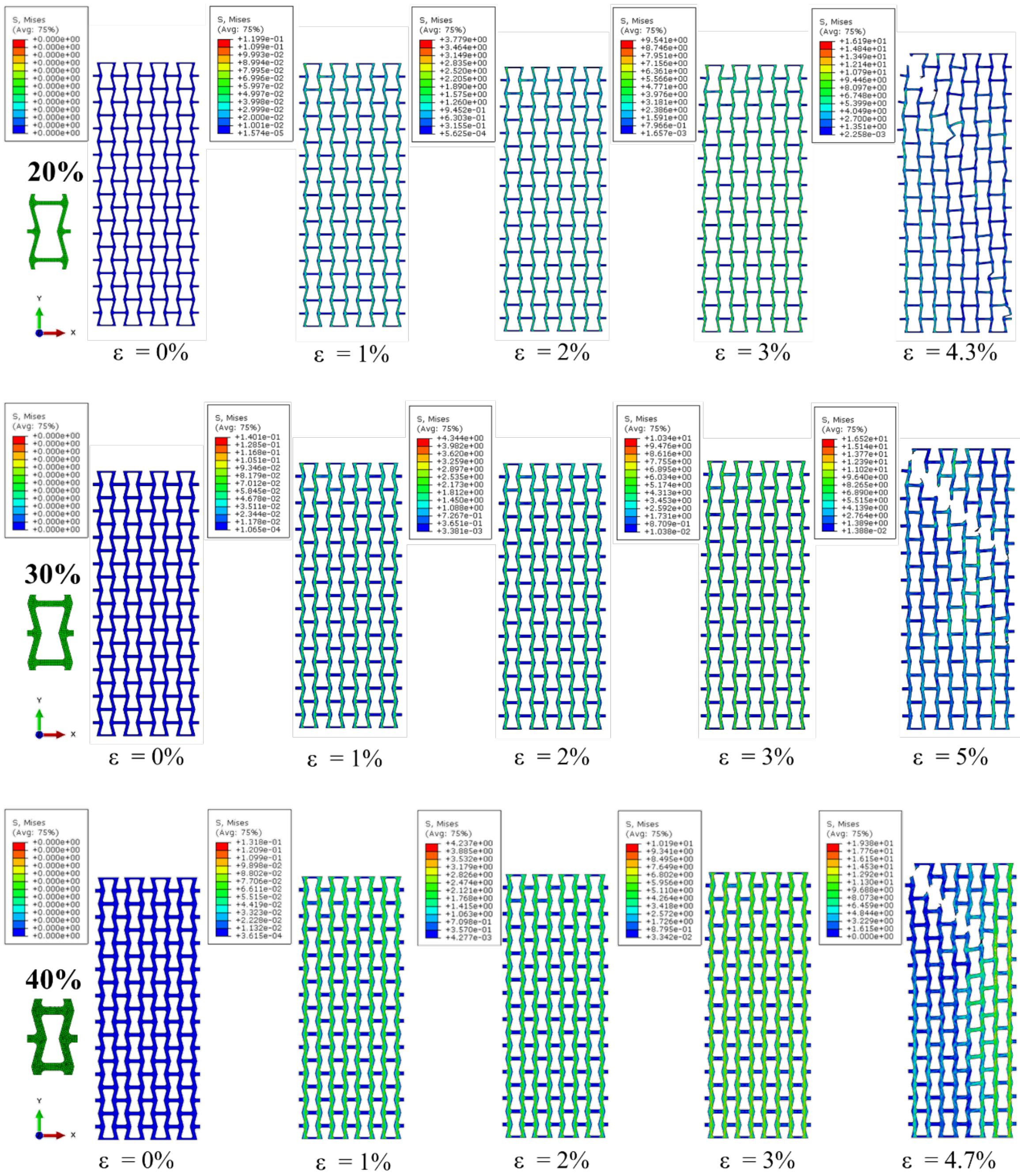

Figure S5. FE contour plots of the von Mises stress (in MPa) induced in the Re-entrant lattice structures at various levels of tensile strain; results are presented for three choices of relative density (20%, 30%, and 40%).

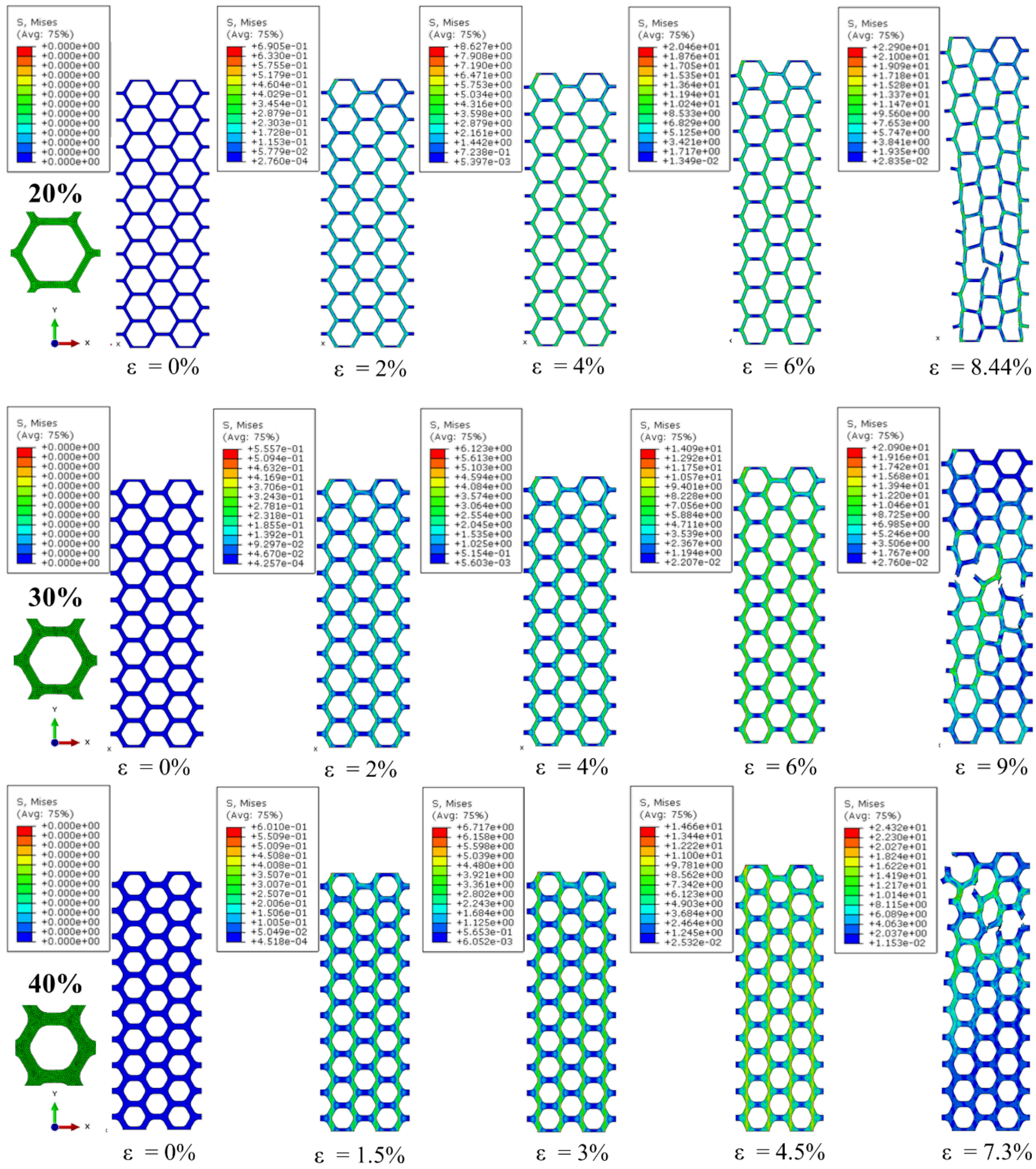

Figure S6. FE contour plots of the von Mises stress (in MPa) induced in the Hexagonal lattice structures at various levels of tensile strain; results are presented for three choices of relative density (20%, 30%, and 40%).

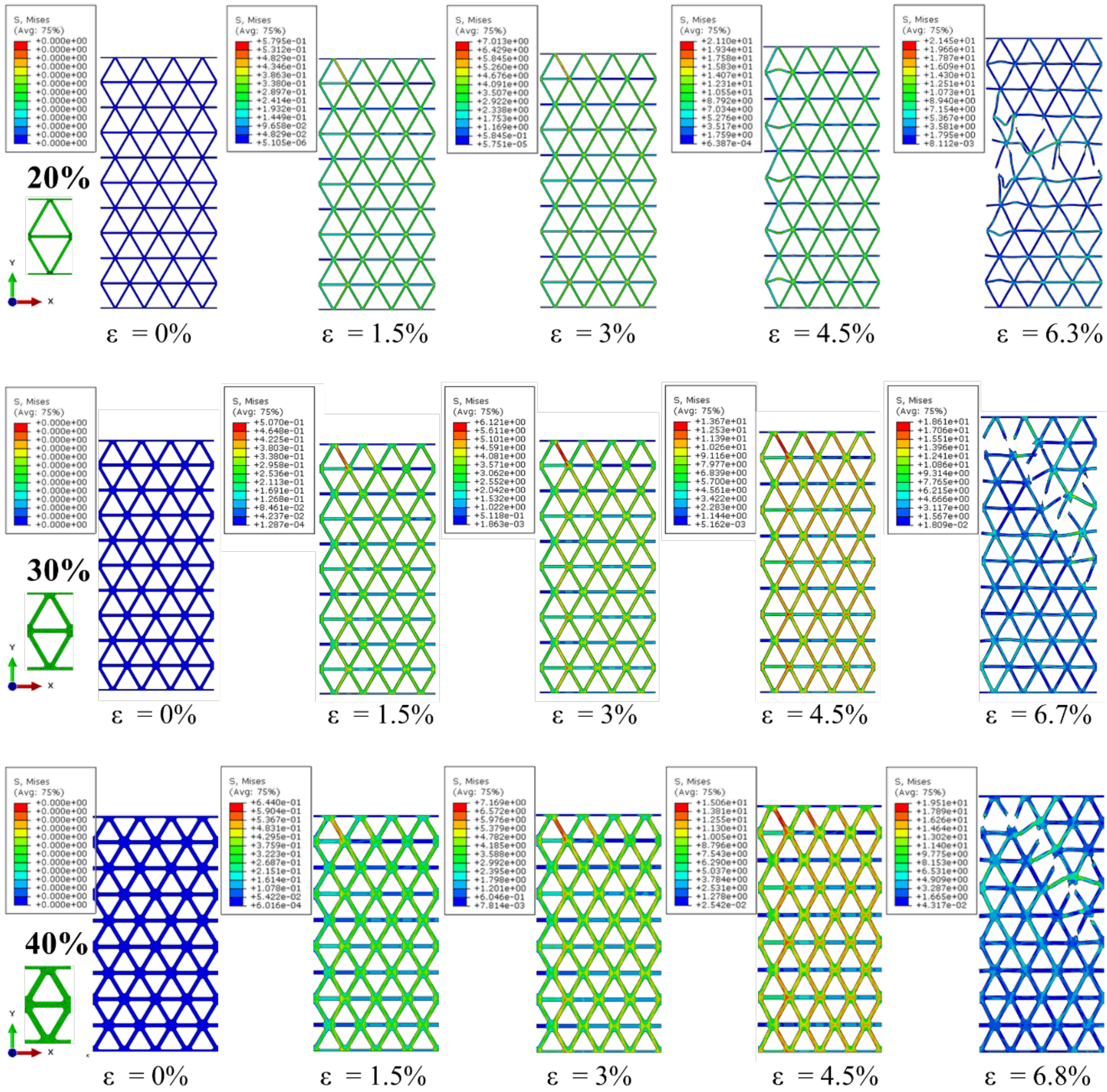

Figure S7. FE contour plots of the von Mises stress (in MPa) induced in the Triangular lattice structures at various levels of tensile strain; results are presented for three choices of relative density (20%, 30%, and 40%).